Volume 18, Number 5, 2025. pp. 597-611

Jordan Journal of Physics

ARTICLE

Magnetothermal Properties of Exciton In TMD_ WS_2 Monolayer

Reham Reda Kmail[a], **Muayyad Abu Saa**[a] and **Mohammad K. ElSaid**[b]

[a] *Physics Department, Arab American University of Jenin (AAUJ), Jenin, West Bank, Palestine.*

[b] *Physics Department, An-Najah National University (ANNU), Nablus, West Bank, Palestine.*

Doi: **https://doi.org/10.47011/18.5.4**

Received on: 16/08/2024; *Accepted on: 16/02/2025*

Abstract: The Hamiltonian of an exciton in a thin layer of WS_2-transition metal dichalcogenide (TMD) was solved by the 1/N expansion method, and the corresponding exciton bound-state energies were obtained. The Hamiltonian describes an electron-hole particle system interacting through an attractive Rytova-Keldysh potential (V_{RK}) in a sheet of WS_2, which is presented in an external uniform magnetic field applied perpendicular to the material sheet plane. We used the computed eigenenergies to calculate the partition function, which depends on the temperature and magnetic field. We calculated the magnetic and thermal quantities of WS_2 TMD material sheet for various values of magnetic field strength and temperature range. The comparisons show that the calculated exciton energy spectra against experimental and theoretical corresponding results are in very good agreement. We have displayed the dependence of magnetization, susceptibility, entropy, and heat capacity as a function of magnetic field and temperature. The paramagnetic behavior of materials over a wide range of magnetic fields was considered. In addition, the density of states (DOS) of TMD-WS_2 material was calculated, and the resulting DOS plot shows an oscillator peak behavior for various ranges of the magnetic field strengths.

Keywords: TMD material, Exciton, 1/N expansion, Magnetic susceptibility, Heat capacity, Entropy, Density of states.

1. Introduction

Transition metal chalcogenide dimers (TMDC or TMD) monolayers are atomically thin MX_2-type semiconductors, where M denotes a transition metal atom (such as Mo or W), and X represents a chalcogen atom (S, Se, or Te). One layer of M atoms is sandwiched between two layers of X atoms. They are part of a large family of so-called two-dimensional materials [1]. Monolayers of MoS_2, WS_2, $MoSe_2$, WSe_2, and $MoTe_2$ exhibit direct bandgaps, and can be used in electronics as transistors and in optics as emitters and detectors. [2-5]. Their two-dimensional nature, combined with strong spin–orbit coupling, makes TMD layers particularly attractive for advanced electronic and spintronic applications [6]. Basically, when a positive hole (an empty electron particle in the valence band) and an electron combine and can move freely through a non-metallic crystal as a unit, the mixing of these two particles is called an exciton. Excitons play an important role in transition metal chalcogenide (TMD) monolayers.

The two-dimensional nature and high spin-orbit coupling of TMD layers render them useful for electronic applications [7]. Work on and use of TMD monolayers is an important research and development area for potential applications in electronics. TMDs are combined with 2D materials such as graphene and hexagonal boron nitride to make van der Waals heterostructures. This is to work on optimizing these heterogeneous structures for use as building blocks for many different devices, such as transistors, solar cells, LEDs, photodetectors, fuel cells, photocatalysts, and sensors. We need to use these devices in our daily lives so that

Corresponding Author: Reham Reda Kmail **Email**: reham.kmail@aaup.edu

they become smaller, cheaper, and more efficient by using single layers [8, 9].

In recent years, the study of excitons in (TMD) monolayers has attracted much attention because their presence has a significant positive impact on the performance of semiconductor devices and their electrical, optical, and transport properties. TMD have emerged as an ideal material platform for exploring the phenomenon of exciton transfer in the works of Malic, Perea-Causin, Rosati, Erkensten**,** and Samuel Brem [10-12]. In many scientific researches, many authors have solved the Schrödinger equation for a quantum dot (QD) in the presence of a constant magnetic field. Elsaid used the 1/N expansion method to calculate the energy states of an electron bound to the donor impurity in the presence of a magnetic field of arbitrary strength. [13-15]. The 1/N expansion method is an effective technique used by many authors, including Shiau, Frenkel, and others, to solve many Hamiltonian bound state systems in reduced dimensions [16-19]. For example, Wannier, Gregory *et al*. [20-22] studied the Hamiltonian quantum dot using this method. Also, Al-Hayek used the 1/N shifted expansion method to calculate the binding energy and energy of the donor impurities with Gaussian confinement in the quantum dot. The 1/N method is considered one of the most powerful and successful methods for solving the Schrödinger equation for the spherical analog potential, and it is used in various branches of theoretical physics. Using this method, we obtain accurate results for calculations of the eigenenergy values of the system, without dealing with path wave functions. Motivated by these studies, the present work applies the shifted 1/N expansion method to solve the exciton Hamiltonian for a thin WS_2 TMD material.

In this work, we investigate the electronic energy spectra, magnetic and thermal properties, the density of states (DOS), and the magnetocaloric effect (MCE) of the exciton system made from an atomic sheet of TMD (WS_2), presented in a magnetic field. All these thermal and magnetic quantities are calculated from the statistical partition function and the well-known statistical relations.

The rest of this work is organized as follows. The Hamiltonian and Schrödinger equation for 2D electron-hole particles in a single-layer interacting TMD, which interact through an attractive Rytova-Keldysh potential, solved by the 1/N- expansion method, is presented in II, the Theory and calculation method Section. In Section III, Results and Discussion, the energy spectra values obtained by 1/N are presented against the magnetic field, discussed, and compared with other studies. This section also examines thermomagnetic quantities, including heat capacity Cv, entropy (S), magnetization (M), susceptibility(X), and magneto-caloric effect (MCE), as well as the density of energy of states (DOS) of the nanosheet TMD -WS_2 material. The conclusion is presented in the final Section.

2. Theory and Method of Calculation

The Hamiltonian for electron and hole particles interacting through an attractive 2D non-Coulombic potential type is used. The model of a system has an exciton with effective mass m* and charge e, moving in a two-dimensional (2D) plane under the influence of a uniform magnetic field applied perpendicular to the monolayer. The corresponding Schrodinger equation is given as [23]:

$$\hat{\mathrm{H}}\psi(x,y) = E\psi(x,y) \tag{1}$$

$$\hat{\mathrm{H}} = -\frac{1}{2}\left(\frac{d^2}{dx^2}+\frac{d^2}{dy^2}\right) - \frac{i}{2}\gamma\left(x\frac{d}{dy} - y\frac{d}{dx}\right) + \frac{1}{8}\gamma^2(x^2+y^2) + V_K(r,\alpha) \tag{2}$$

where: $r = \sqrt{x^2+y^2}$.

Where γ, a dimensionless magnetic parameter, is related to the magnetic field.

$V_K(r,\alpha)$ is the Rytova-Keldysh type potential.

The nonlocally screened electron–hole interaction in two-dimensional systems, such as monolayer transition metal dichalcogenides (TMDs), is described by the Rytova–Keldysh potential [23]:

$$V_{RK}(r) = -\frac{e^2}{8\varepsilon_0 r_0}\left[H_0\left(\frac{kr}{r_0}\right) - Y_0\left(\frac{kr}{r_0}\right)\right] \tag{3}$$

where:

H_0 and Y_0 are zero-order Struve and Bessel functions, respectively;

r_0 is related to the screening length related to the 2D polarizability of the monolayer material;

ε_0 is the vacuum permittivity;

k is the average dielectric constant for the surrounding material;

α is the parameter for characterizing potential and is defined as $\alpha = r_0/ka_0^*$, where a_0^* is the effective Bohr radius.

This potential describes two charges in the electrostatic interaction for thin semiconductor and semi-metal films, predicted by Rytova-Keldysh and then discussed in many research works [24, 25].

The Hamiltonian, Eq. (2), of the system after adding Rytova-Keldysh potential, Eq. (3), is given as:

$$\hat{\mathrm{H}} = -\frac{1}{2}\left(\frac{d^2}{dx^2}+\frac{d^2}{dy^2}\right) - \frac{i}{2}\gamma\left(x\frac{d}{dy} - y\frac{d}{dx}\right) + \frac{1}{8}\gamma^2 r^2 - \frac{e^2}{8\varepsilon_0 r_0}\left[H_0\left(\frac{kr}{r_0}\right) - Y_0\left(\frac{kr}{r_0}\right)\right] \quad (4)$$

The analytic solution of the Hamiltonian in Eq. (4) is not attainable. We found that 1/N-expansion is an effective and accurate technique in solving the Hamiltonian given by Eq. (4).

We can write the radial part of the Schrödinger equation in N-dimensional space as follows:

$$\left(-\frac{\hbar^2}{2m^*}\left(\frac{d^2}{dr^2}+\frac{N-1}{r}\frac{d}{dr}\right) + \frac{l(l+N-2)\hbar^2}{2m^* r^2} + V(r)\right)\emptyset(r) = E\emptyset(r) \quad (5)$$

where m^* is the electron effective mass, e is the charge of the electron, ħ is related to the Planck constant, and N is the number of dimensions. $l = |m_l|$, where $|m_l|$ is the magnetic quantum number $(m_l = 0, \pm1, \pm2, \pm3, \ldots)$ that labels the quantum dot (QD) energy states and appears in the term $l(l+N-2)$.

By using the parameter $k, \bar{k} = k - a = N + 2l - a$, we can rewrite Eq. (5) to become:

$$\left(-\frac{\hbar^2}{2m^*}\frac{d^2}{dr^2} + \bar{k}^2\left((\hbar^2\left(1-\frac{1-a}{\bar{k}}\right)(1-3-a)/\bar{k})\right)/8m^* r^2 + V(r)/Q\right)\emptyset(r) = E\emptyset(r) \quad (6)$$

where $Q = \bar{k}^2$ is a scaling constant used to make Eq. (5) and Eq. (6) equivalent.

We can use the parameter $\bar{k}$ and the shift parameter a to expand the Schrodinger equation to calculate the energy eigenvalues $E(n_r, m_l)$. The complete mathematical steps that lead us to the eigenvalues of QD energy expressions in terms of powers of 1/k̄ are given explicitly in the Appendix. The intrinsic energy values $E(n_r, m_l)$ are in powers of $1/\bar{k}$ and are given as follows: $E(n_r, m_l) = E_0 + E_1 + E_2 + E_2{+}$..... These energy terms are defined in terms of quantum numbers, potential roots (r_0), and derivatives ($V^n(r_0)$) [26, 27].

The shift parameter a is chosen to make a second-order contribution E_1 vanish. In general, the presence of this condition ensures exact analytical energy results with the 1/N method for both the harmonic oscillator and hydrogen Hamiltonian [28, 29].

The Thermodynamic Properties: Heat Capacity (Cv) and Entropy (S)

We evaluate the mean energy, $< E((n_r, m_l, B, T) >$ expression from the partition function Z.

The complete thermodynamic quantities, including heat capacity and entropy, start by evaluating the partition function at any temperature and magnetic field strength [30]:

$$< Z >= \sum_{j=1}^{i} e^{-E_j/K_B T} \quad (7)$$

where K_B is the Boltzmann constant, T is the temperature, j is the index for the microstates of the system, and E_j is the total energy of the system in the respective microstate.

$$< E >= \frac{\sum_{j=1}^{i} E_j e^{-\frac{E_j}{K_B T}}}{\sum_{j=1}^{i} e^{-\frac{E_j}{K_B T}}} \quad (8)$$

The heat capacity C_v is the temperature derivative of the mean energy given as [30]:

$$C_v = \frac{\partial <E>}{\partial T} \quad (9)$$

Similarly, the entropy S of the exciton system can also be computed using the expression

$$S = \frac{\partial(K_B \mathrm{T} \ln <\mathrm{Z}>)}{\partial \mathrm{T}} \quad (10)$$

The Magnetic Properties: Magnetization (M) and Susceptibility (χ)

The magnetization (M) is defined as the negative derivative of the average energy of the two-dimensional exciton system with respect to the magnetic field strength BBB [30]:

$$M = -\frac{\partial <E>}{\partial B} \quad (11)$$

where $< E >$ is the average energy of the exciton system in the magnetic field (B).

The magnetic susceptibility χ is obtained by differentiating the magnetization with respect to the magnetic field strength [30]:

$$\chi = \frac{\partial M}{\partial B} \quad (12)$$

The Density of States (DOS):

The DOS of the exciton system of TMD-WS_2 material is another property that can reveal important information about the electronic structure of nanomaterials. It is expressed as the sum of a series of delta functions, given by [31, 32]:

$$DOS(E) = \frac{1}{A}\sum_{n=1}^{N} \delta(E - E_n) \quad (13)$$

The delta function can be replaced by a more practical computation Gaussian distribution as:

$$DOS(E) = \frac{1}{\sqrt{2\pi\Gamma^2}}\sum_n \exp\left[\frac{-(E-E_n)^2}{2\Gamma^2}\right] \quad (14)$$

where Γ is the broadening factor, E_n is the eigenenergy of the exciton system, which was calculated by the 1/N expansion method, and A is the area of the material sample [32].

The Magneto-Caloric Effect (MCE)

The magnetocaloric effect (MCE) is defined as the change in the entropy of the system, $\triangle S_m$, as a response to the change in the magnetic energy of the exciton system presented in an applied magnetic field, given as [33, 34]:

$$\Delta S_m = S(T_0, B_{=0}) - S(T_0, B_{\neq 0}) \quad (15)$$

where:

ΔS_m is magnetic entropy change (eV/K);

S_m is magnetic entropy;

T_0 is temperature;

$B_{=0}$ is the magnetic field equal to zero;

$B_{\neq 0}$ is the magnetic field not equal to zero.

3. Results and Discussion

In this part, the computed physical quantities will be listed in tables and displayed in figures. The discussion of the results consists of two main steps. In the first step, the accuracy of the energy spectra obtained using the 1/N expansion method is evaluated by comparison with previously reported experimental and theoretical results. In the second step, these excitonic results are used to explain the dependence of the magnetothermal properties, DOS and MCE of the WS_2 material as the magnetic field strength changes to include a strong range, B=60 T.

The physical parameters used for WS_2, in numerical computations are: the effective mass of an electron $m^* = 0.16m_e$, the average dielectric constant of the material $k = 1$, the effective screening length of the monolayer $r_0 = 75A^{\circ}$, and the effective Bohr radius $a = 3.779$. [23]

Tables 1.a-1.c list the results computed using the 1/N expansion method and compare them with the reported results in Ref. [23]. The quantitative comparison demonstrates the accuracy of the 1/N expansion method over the entire range of magnetic field strengths.

TABLE 1.a. Ground-state energies (1s, 2s) (in eV) at different magnetic field strengths (in T in the present work and in units of γ in Ref [23], where γ = 0.01 corresponds to a magnetic field B = 60.16T) for WS_2, calculated using the 1/N-shift expansions method and compared with the reported results in Ref. [23].

WS_2		1s $\|1,0>$		2s $\|2,0>$	
B(T)	Γ	E (present work) (eV)	E(Ref [23]) (eV)	E (present work) (eV)	E (Ref[23]) (eV)
0.00	0.00000	-0.3179	-0.3187	-0.1523	-0.1516
7.52	0.00125	-0.3179	-0.3184	-0.1520	-0.1513
15.0	0.00250	-0.3178	-0.3186	-0.1514	-0.1507
30.0	0.00500	-0.3175	-0.3179	-0.1488	-0.1478
45.1	0.00750	-0.3170	-0.3178	-0.1446	-0.1436
60.1	0.01000	-0.3163	-0.3128	-0.1392	-0.1378
150	0.02500	-0.3086	-0.3094	-0.0888	-0.0853
300	0.05000	-0.2854	-0.2862	0.0303	0.0339
601	0.10000	-0.2188	-0.2188	0.3092	0.3106
3008	0.50000	0.5246	0.5259	2.7905	2.9713
4512	0.75000	1.0328	1.0344	4.3861	4.3874
6016	1.00000	1.5568	1.5525	5.9913	5.9938

TABLE 1.b. Ground-state energies (3s, 4s) (in eV) at different values of magnetic field strength (in a unit of T in present work and a unit of γ in Ref [23], where γ = 0.01 corresponds to a magnetic field of B = 60.16T) for WS_2, calculated using the 1/N-shift expansions method, compared with the reported results in Ref. [23].

WS_2		3s $\|3,0>$		4s $\|4,0>$	
B (T)	Γ	E (present work) (eV)	E (Ref [23]) (eV)	E (present work) (eV)	E (Ref[23]) (eV)
0.00	0.00000	-0.0952	-0.0944	-0.0657	-0.0648
7.52	0.00125	-0.0944	-0.0936	-0.0639	-0.0631
15.0	0.00250	-0.0922	-0.0909	-0.0591	-0.0579
30.0	0.00500	-0.0843	-0.0827	-0.0439	-0.0404
45.1	0.00750	-0.0730	-0.0700	-0.0227	-0.0178
60.1	0.01000	-0.0591	-0.0552	0.0027	0.0074
150	0.02500	0.0562	0.0596	0.1868	0.1872
300	0.05000	0.2868	0.2886	0.5277	0.5285
601	0.10000	0.7839	0.7845	1.2436	1.2408
3008	0.50000	5.0074	5.0114	7.2089	7.2151
4512	0.75000	7.6905	7.6978	10.979	10.993
6016	1.00000	10.383	10.392	14.759	14.777

TABLE 1.c. Ground-state energies (5s, 6s) (in a unit of eV) at different values of magnetic field strength (in a unit of T in present work and a unit of γ in Ref [23], where γ = 0.01 corresponds to a magnetic field B = 60.16T) for WS_2, calculated using the 1/N-shift expansions method, compared with the reported results in Ref. [23].

WS_2		5s $\|5,0>$		6s $\|6,0>$	
B (T)	γ	E (present work) (eV)	E (Ref [23]) (eV)	E (present work) (eV)	E (Ref[23]) (eV)
0.00	0.00000	-0.0481	-0.0474	-0.0367	-0.0361
7.52	0.00125	-0.0448	-0.0439	-0.0312	-0.0300
15.0	0.00250	-0.0366	-0.0304	-0.0196	-0.0156
30.0	0.00500	-0.0119	-0.0069	0.0180	0.0226
45.1	0.00750	0.0220	0.0261	0.0642	0.0674
60.1	0.01000	0.0595	0.0631	0.1132	0.1158
150	0.02500	0.3109	0.3121	0.4312	0.4310
300	0.05000	0.7616	0.7619	0.9917	0.9883
601	0.10000	1.6961	1.6937	2.1446	2.1421
3008	0.50000	9.4029	9.4133	11.592	11.581
4512	0.75000	14.260	14.276	17.537	17.559
6016	1.00000	19.127	19.153	23.491	23.524

In addition, energy values at different quantum levels (| n,m>) were calculated for the same field values that were defined in the previous tables in order to make the work more comprehensive. We changed the quantum state from $< s >$ to $< p >$ to see how energy essentially depends on these values and to see the changes that occur in energy at these quantum numbers, as shown in Table 2.

TABLE 2. Ground-state energies (in a unit of eV) at different values of magnetic field strength (in a unit of T in the present work and unit of γ in Ref [23], where γ = 0.01 corresponds to the magnetic field B = 60.16T) for WS_2, calculated using the 1/N-shift expansions method.

WS_2		1p	2p	3p	4p	5p	6p
		|1,1 >	|2,1 >	|3,1 >	|4,1 >	|5,1 >	|6,1 >
B(T)	γ	E(eV)	E(eV)	E(eV)	E(eV)	E(eV)	E(eV)
0.00	0.00000	-0.1843	-0.1098	-0.0739	-0.0532	-0.0401	-0.0313
7.52	0.00125	-0.1815	-0.1065	-0.0698	-0.0477	-0.0326	-0.0213
15.0	0.00250	-0.1784	-0.1023	-0.0633	-0.0378	-0.0188	-0.0027
30.0	0.00500	-0.1717	-0.0912	-0.0451	-0.0106	0.0195	0.0481
45.1	0.00750	-0.1640	-0.0773	-0.0220	0.0236	0.0657	0.1058
60.1	0.01000	-0.1557	-0.0614	0.0040	0.0611	0.1146	0.1660
150	0.02500	-0.0944	0.0517	0.1883	0.3123	0.4324	0.5502
300	0.05000	0.0299	0.2879	0.5289	0.7627	0.9927	1.2201
601	0.10000	0.3095	0.7848	1.2444	1.6969	2.1453	2.5911
3008	0.50000	2.7907	5.0073	7.2089	9.4030	11.592	13.779
4512	0.75000	4.3861	7.6903	10.979	14.260	17.537	20.811
6016	1.00000	5.9912	10.382	14.759	19.127	23.491	27.852

In Figs. 1(a) and 1(b), for the sake of more qualitative comparisons, the tabulated energy values are also displayed against the magnetic field for different s-states. The effect of magnetic field confinement on the ground-state energies is illustrated. The figures show that the first level is not affected by an increase in the magnetic field, as it maintains an almost constant value. However, for higher energy levels, a noticeable dependence on the magnetic field is observed, with the energy values increasing as the magnetic field strength increases. This is completely consistent with the results of Ref. [23]. Comparing the two figures, we can see a good match between the two works.

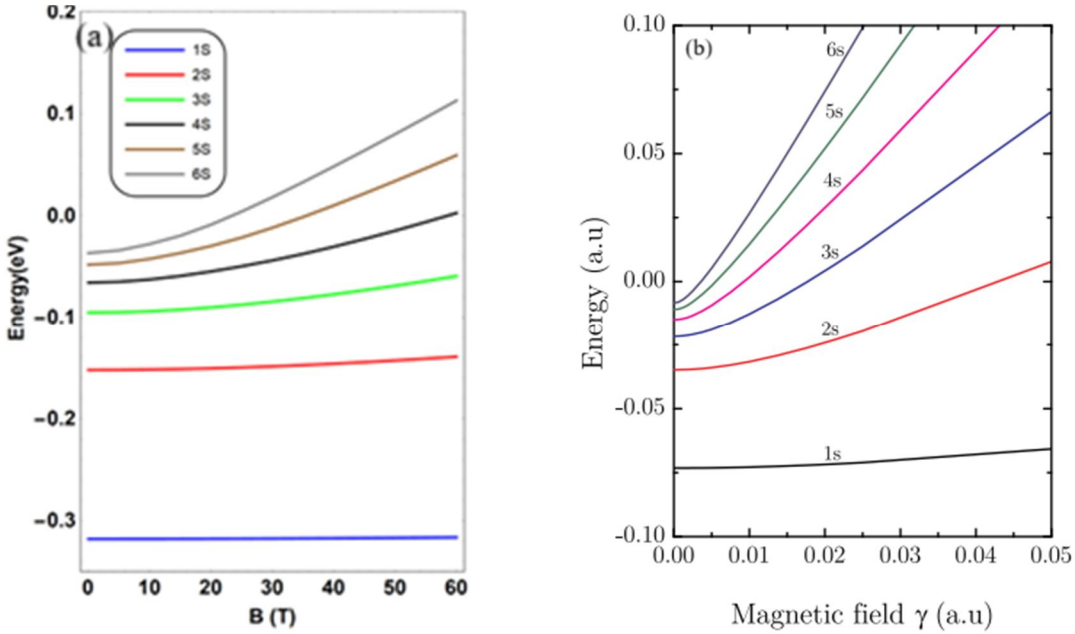

FIG. 1. Ground-state energy as a function of magnetic field for WS_2. Figures are taken from Ref. [23]. Different systems of energy and magnetic field units are used in both plots. (a) present work, (b) Ref. [23]. The two figures have different scales, where γ = 0.01 corresponds to the magnetic field of B = 60.16T.

Figure 2 shows the influence of the magnetic field effect on the ground-state energies for higher quantum p-states labelled by magnetic quantum number m. As the magnetic field increases, the energy values also increase.

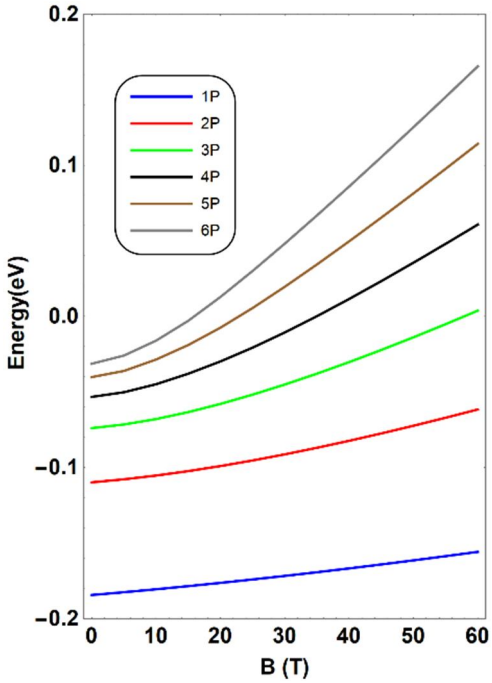

FIG. 2. Ground-state energy <E> as a function of magnetic field (B) on the ground-state energies for quantum number (p) of WS_2.

Next, we studied the ground state energy as a function of temperature at different values of the magnetic field. As shown in Fig. 3, when we turn off the magnetic field (B = 0T), we find that the average energies increase with increasing temperature. In addition, the average energy convergence is achieved as we increase the number of exciton states from 15 to 20.

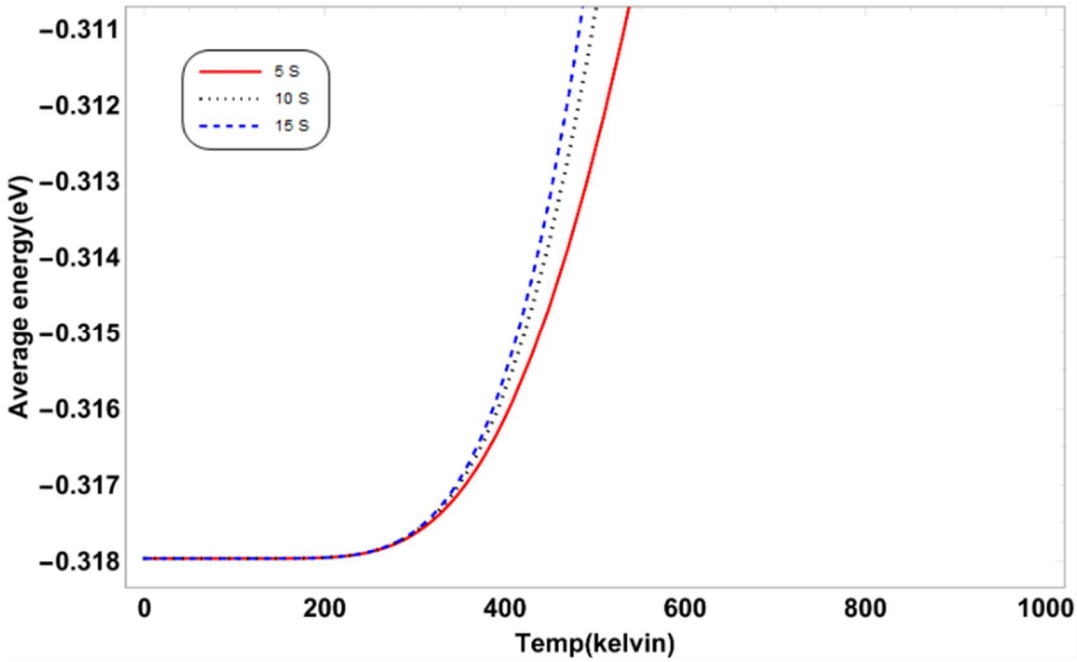

FIG. 3. Average energy as a function of temperature when we turn off the magnetic field (B=0T) for WS_2, computed for different numbers of S-states.

In Fig. 4, we now switched on the magnetic field and tested again the convergence of the average energy of the exciton system against the temperature, calculated at fixed magnetic field strength, $B \approx 60\,T$, and various numbers of bases. The figure clearly shows a very good convergence behavior of the average energy for taking only 15 bases of exciton S-states.

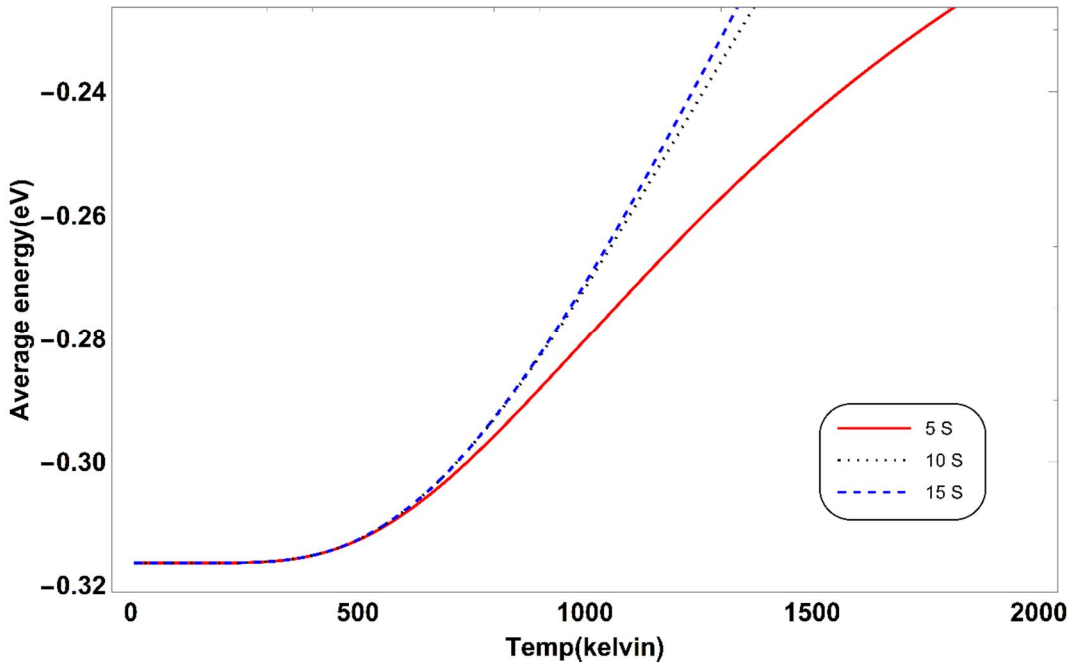

FIG. 4. Average energy ∈ as a function of temperature (T) when we switched the magnetic field (B = 60.16T) for different numbers of S-states for WS_2.

The dependence of the heat capacity on temperature and magnetic field for the WS_2 sheet is shown in Fig. 5. For the zero magnetic field case (B = 0), the heat capacity increases with temperature, reaching a peak value, known as the Schottky anomaly, at $C_v/k_B \approx 2.4$ at 1000^0 K. The heat capacity starts decreasing until it reaches almost asymptotic zero value at T≈3000K for WS_2. In the presence of a strong magnetic field B $\approx 60\,T$, the exciton becomes more confined, and the exciton heat capacity reaches a peak value of approximately 1.8 at 1200K.

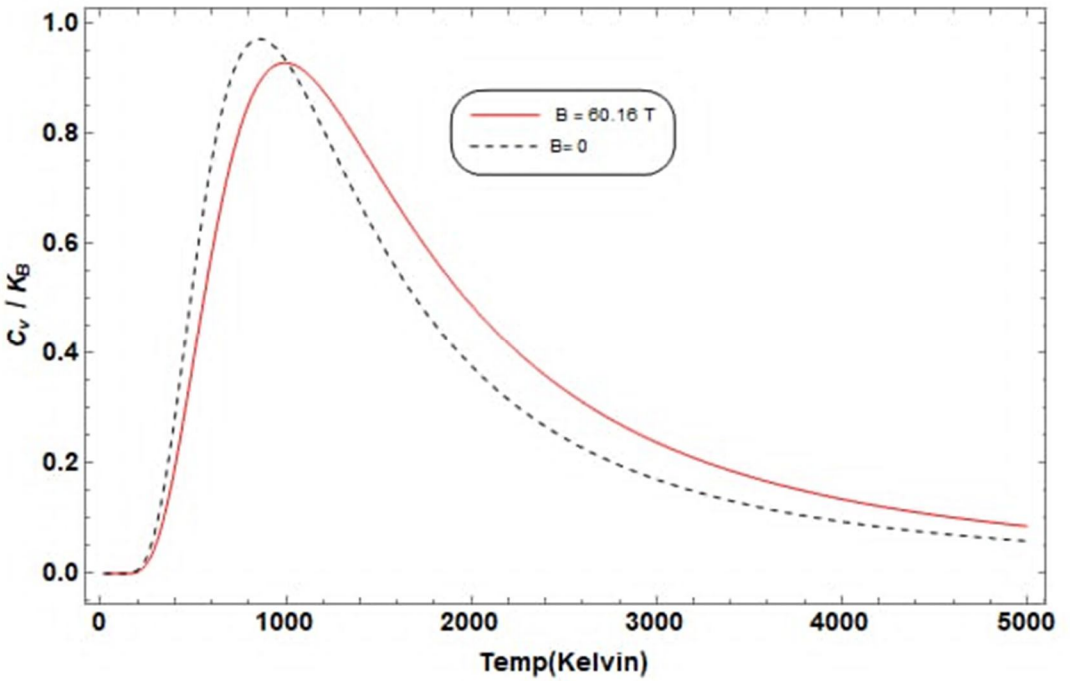

FIG. 5. Heat capacity as a function of temperature and magnetic field for WS_2.

Figure 6 shows the entropy as a function of temperature and magnetic field. The plot shows that the entropy increases with increasing temperature until it reaches a saturation entropy limit of $S/k_B \approx 1.7$ for zero magnetic field at

3000 K, and 1.6 at 60.16 T at the same temperature. We reduced the temperature to 2000^0 K to see the stability of entropy in the sub-figure for both cases, with and without a magnetic field.

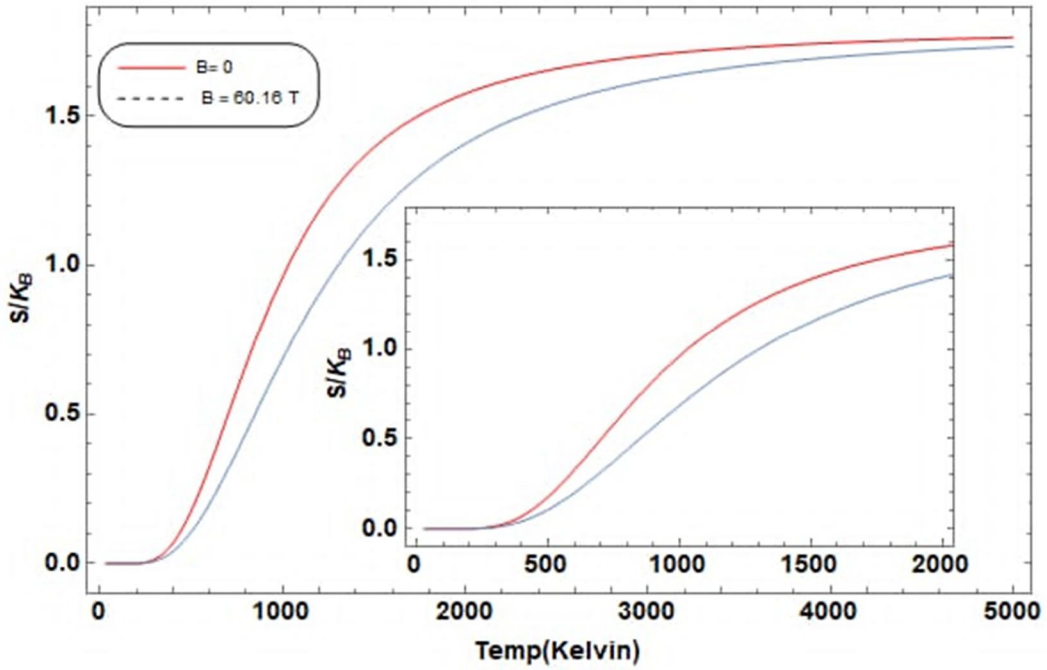

FIG. 6. Entropy as a function of temperature for different magnetic field strengths for WS (the inset figure is plotted for the low temperature range).

Magnetic properties were also studied, starting with the computation of statistical energy for WS_2 under the effect of temperature and magnetic field. The statistical energy, shown in the present work for WS_2 in Fig. 7, is calculated at 100 K and 300 K for a magnetic field range from 0 to 60 T. The statistical energy is found to reach -0.318 eV at 100 K and -0.317 eV at 300 K.

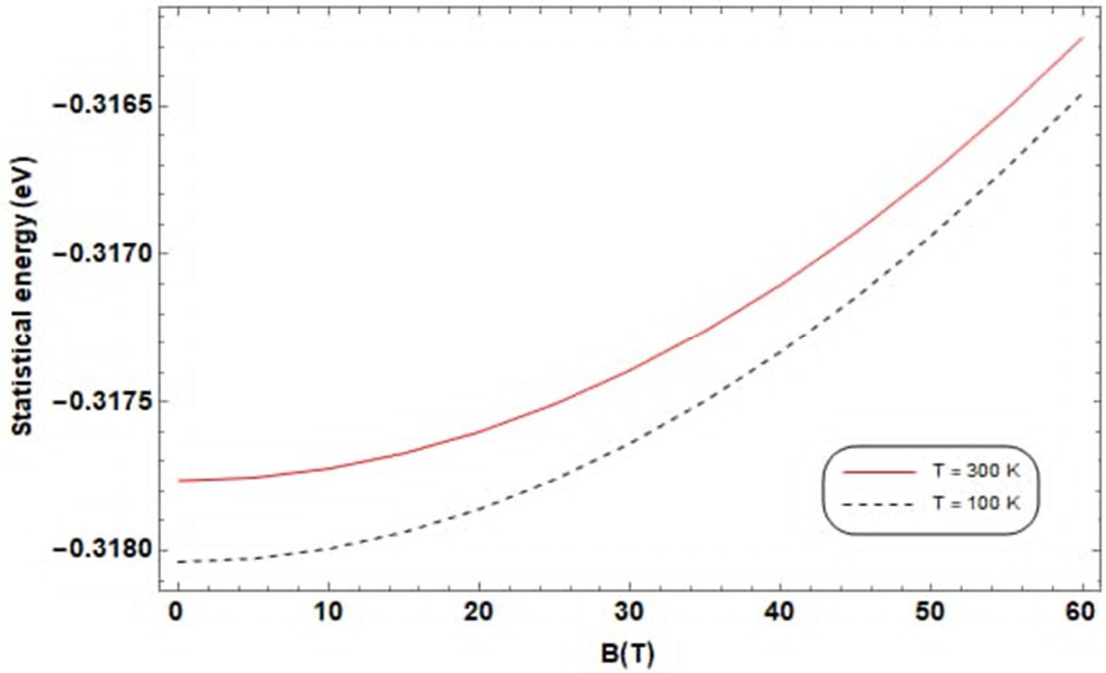

FIG. 7. Statistical energy as a function of magnetic field for WS_2.

We have calculated the magnetization in units of effective Bohr magneton [35], $\mu_B = e\hbar/2m^* = 0.3622*10^{-3}$ eV/T, for WS_2. Also, we studied the magnetization as a function of magnetic field at different values of temperature. Figure 8 shows that the magnetization curve

decreases with increasing magnetic field, starting from zero at 0 T to reach -0.05 at 60 T at 900 K.

When we decreased the temperature to 10 K, the magnetization reached -0.14 at 60 T, see Fig. 8. This means that, when we decrease the temperature, the magnetization increases at high magnetic fields (60 T), but at low magnetic fields (0 T) the magnetization takes the same value and starts from zero.

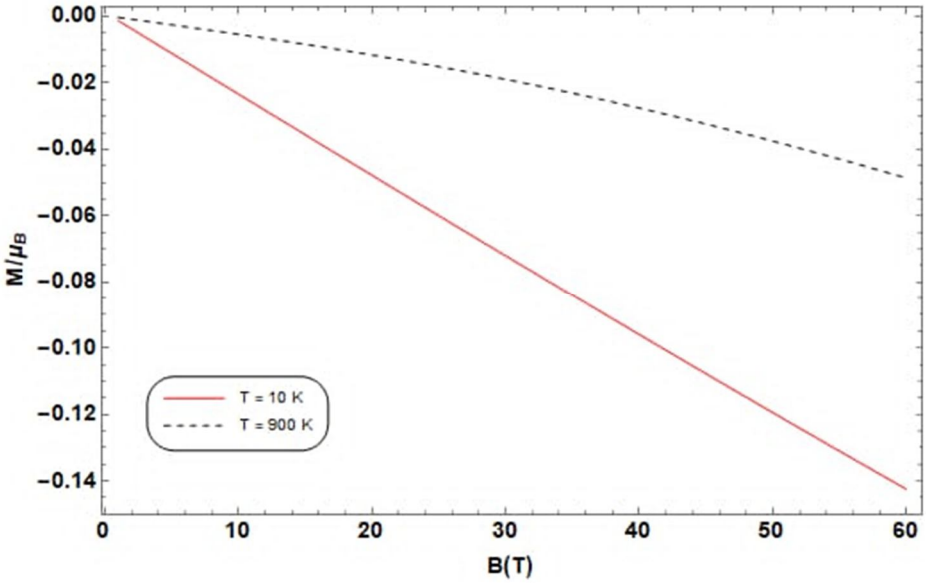

FIG. 8. Magnetization as a function of magnetic field at 900 K and 10 K for WS_2.

In Fig. 9, we studied the behavior of computed magnetic susceptibility for both low and high temperature ranges in the presence of a magnetic field for WS_2. The results are displayed for temperatures of 10 K and 150 K.

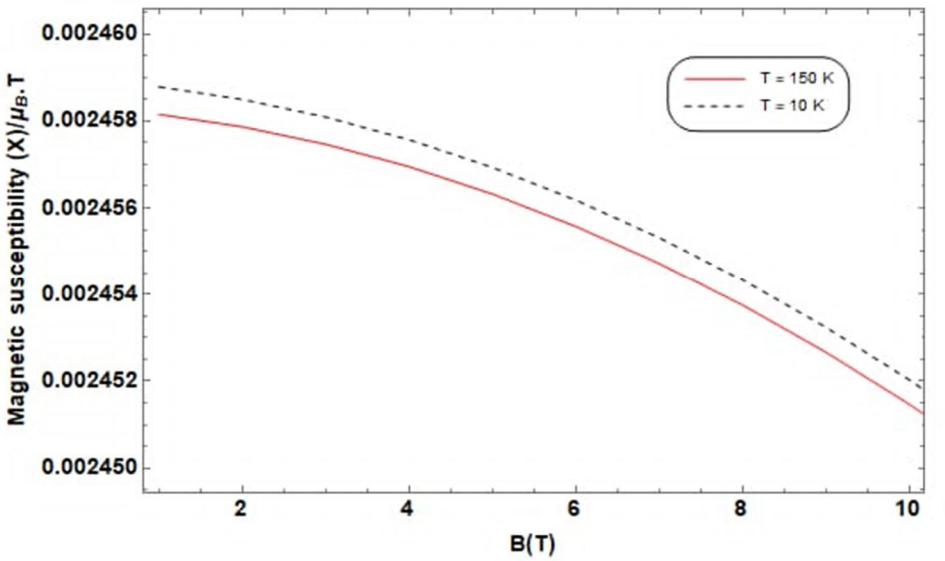

FIG. 9. Magnetic susceptibility as a function of a magnetic field at 10 K and 150 K for WS_2.

The density of states (DOS) is a significant physical quantity to reveal information about the electronic properties of materials, by describing the system's responses to Hamiltonian parameters, such as the magnetic field and confinement potential.

In Fig. 10, the DOS is plotted as a function of energy at different values of the magnetic field (50 T, 60.16 T). The plot for WS_2 below shows that the presence of the external magnetic field removes the degeneracy of the states, so the DOS gives one at each value of the energy spectrum. We observe that as the magnetic field strength increases, the Landau level energy separation $\hbar\omega_c$ also increases, leading to a reduction in the number of LL-states in the DOS

of WS_2 material. For example, the number of states (3 states) at B = 60 T (black color, dashed plot) is smaller than the number of states (4 states) for a lower magnetic field strength (red color, solid line plot) and for a fixed energy range (E).

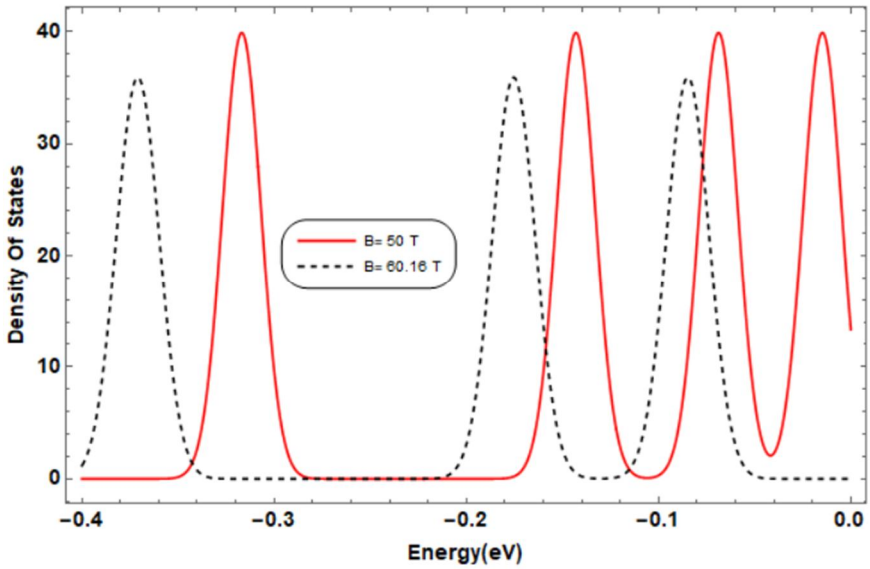

FIG. 10. DOS vs. energy for WS_2 at different magnetic field values.

The magnetocaloric effect (MCE) was studied in order to identify the thermomagnetic properties by investigating the behavior of the material with the temperature changes when the material is exposed to a changing magnetic field. Our study is devoted to a sheet made from TMD materials (WS_2). The MCE, represented by ΔS against the temperature T, shows a Gaussian distribution. A high temperature is required to see the MCE in TMD since the binding energy for an exciton in a strong magnetic field is very large, and thus more thermal energy is needed to be absorbed by the exciton. We observe that this temperature is far from the room temperature range, as TMD materials require very high thermal energy (E_{th}) in order to increase the kinetic energy (K) of the electron. Under these conditions, the exciton system transitions randomly between states, producing the observed entropy variation, as shown in Fig. 11 [36, 37].

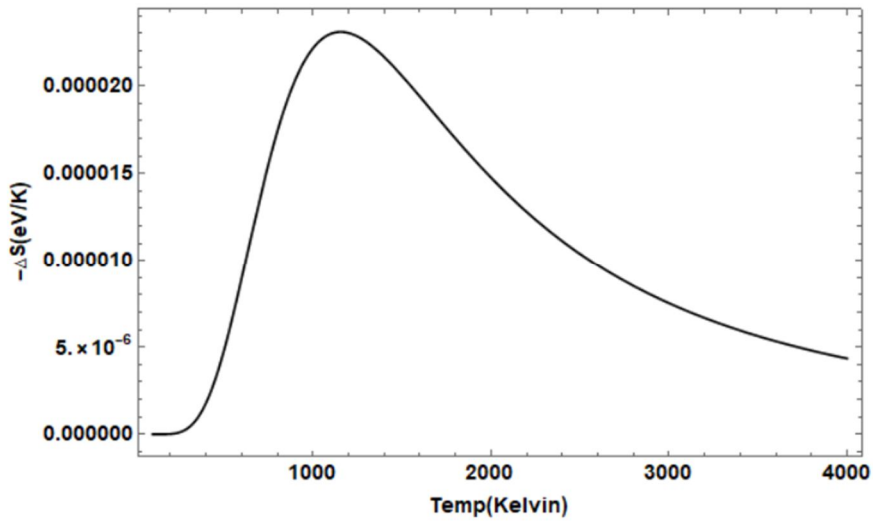

FIG. 11. MCE vs temperature for WS_2 at different magnetic field values, $\Delta S_m = S(B_{=60.16}) - S(B_{=0})$.

4. Conclusions

In conclusion, we have investigated the magnetothermal properties of WS_2 TMD material. Additionally, we have studied the DOS and MCE of the same material as functions of the magnetic field. The Schrödinger equation for the exciton system in a magnetic field was solved by using the shifted 1/N expansion method to find the eigenenergy states. We have

tested the computed results by the 1/N method against different computation results calculated by various numerical methods. The results show that the 1/N method is both accurate and effective for solving the exciton Hamiltonian system with a spherically symmetric potential such as V_{RK}. We have ensured the convergence issue of the statistical energy by varying the number of states in each computation step. The behavior of the magnetothermal properties of the exciton system for WS_2 nanosheet had been studied as a function of magnetic field and temperature. The results show that the heat capacity curve exhibits a Schottky anomaly. Furthermore, the magnetic susceptibility curve for WS_2 was calculated and displayed. We have calculated the density of the state function, DOS, of the exciton system. The DOS plots show an oscillatory-type behavior for different values of the magnetic field, reflecting the Landau-level (LL) states of the exciton system presented in a magnetic field.

The present study also investigates the MCE of an exciton in TMD material, which is defined as the magnetothermodynamic phenomena that has an application in magnetic refrigeration. We have found that the calculated $\Delta S - T$ plot for the exciton system of the WS_2 monolayer has a Gaussian distribution shape.

This study reveals that the WS_2-TMD material has attractive magnetic and thermal properties, which make WS_2 a very promising material in the next generation of nanoelectronics.

Appendix

Shifted 1/N Expansion Method

The 1/N expansion method is used to solve Eq. (5) systematically in terms of the expansion parameter 1/k̄. At large k̄, the contribution of energy comes from the effective potential:

$$V_{eff} = \frac{\hbar^2}{8m^* r^2} + \frac{V(r)}{Q} \tag{A1}$$

where $Q = k^2$ is a scaling constant. V_{eff} has a minimum value at r_0, so that we have:

$$4m^* r_0^3 V'(r_0) = \hbar^2 Q \tag{A2}$$

To shift the origin of the coordinate system to the position of the minimum of the effective potential, a new variable x is defined:

$$x = \frac{k^{\frac{1}{2}}}{r_0}(r - r_0) \tag{A3}$$

Using a Taylor expansion around the effective minimum r0 (corresponding to x = 0), an analytical equation similar to the Schrödinger equation for a one-dimensional solvable nonharmonic oscillator is obtained. The coefficients of both equations are compared to determine all parameters of the anharmonic oscillator in terms of k̄, Q, r0, and the potential derivatives, allowing the determination of the energy spectrum. The oscillator frequency is then given by:

$$\omega = \frac{\hbar}{2m^*}\left(3 + \frac{r_0 V''(r_0)}{V'(r_0)}\right)^{1/2} \tag{A4}$$

To calculate the energy eigenvalues, the Schrödinger equation is expanded in powers of $1/\bar{k}$, where $\bar{k} = N + 2l - a$, N is the number of spatial dimensions and (a) is the so-called shifted parameter. The shifted parameter a is defined as:

$$a = 2 - \frac{2(2n_r - 1)m^*\omega}{\hbar} \tag{A5}$$

For any values of radial quantum numbers n_r and m_l, the energy eigenvalues $E(n_r, m_l)$ are given by:

$$E(n_r, m_l) = E_0 + E_1 + E_2 + E_3 \tag{A6}$$

where:

$$E_0 = V(r) + \left(\frac{Q}{8 * m^* * r^2}\right)$$

$$E_1 = \frac{(c_1 * c_3)}{(8 * m^*)}$$

$$E_2 = (E_1 + \alpha_1)/r^2$$

$$E_3 = \frac{\alpha_2}{k * r^2}$$

where:

$$Q = (N + 2 * l - a)^2$$

$$c_1 = (1 - a)$$

$$c_2 = (2 - a)$$

$$c_2 = (2 - a)$$

$$c_3 = (3 - a)$$

$$\alpha_1 = n_1 * e_2 + 3 * n_2 * e_4 - c_5 * \left(e_1{}^2 + 6 * n_1 * e_1 * e_3 + n_4 * e_3^2\right)$$

$$\alpha_2 = t_7 + t_{12} + t_{16}$$

$$c_5 = \omega^{-1}$$

The forms of previous parameters are given in the following:

$$t_7 = t_1 - c_5 * (t_2 + t_3 + t_4 + t_5 + t_6)$$

$$t_{12} = c_5^2 * (t_8 + t_9 + t_{10} + t_{11})$$

$$t_{16} = -\, c_5^3 * (t_{13} + t_{14} + t_{15})$$

with:

$$t_1 = n_1 * d_2 + 3 * n_2 * d_4 + 5 * n_3 * d_6$$

$$t_2 = n_1 * e_2{}^2 + 12 * n_2 * e_2 * e_4$$

$$t_3 = 2 * e_1 * d_1 + 2 * n_5 * e_4{}^2$$

$$t_4 = 6 * n_1 * e_1 * d_3 + 30 * n_2 * e_1 * d_5$$

$$t_5 = 6 * n_1 * e_3 * d_1 + 2 * n_4 * e_3 * d_3$$

$$t_6 = 10 * n_6 * e_3 * d_5$$

$$t_8 = 4 * e_1{}^2 * e_2 + 36 * n_1 * e_1 * e_2 * e_3$$

$$t_9 = 8 * n_4 * e_2 * e_3^2$$

$$t_{10} = 24 * n_1 * e_1^2 * e_4 + 8 * n_7 * e_1 * e_3 * e_4$$

$$t_{11} = 12 * n_8 * e_3^2 * e_4$$

$$t_{13} = 8 * e_1^3 * e_3 + 108 * n_1 * e_1^2 * e_3^2$$

$$t_{14} = 48 * n_4 * e_1 * e_3^3$$

$$t_{15} = 30 * n_9 * e_3^4$$

where (n's), (d's), and (e's) are parameters given as:

$$n_1 = 1 + 2 * n_r$$

$$n_2 = 1 + 2 * n_r + 2 * n_r{}^2$$

$$n_3 = 3 + 8 * n_r + 6 * n_r{}^2 + 4 * n_r{}^3$$

$$n_4 = 11 + 30 * n_r + 30 * n_r{}^2$$

$$n_5 = 21 + 59 * n_r + 51 * n_r{}^2 + 34 * n_r{}^3$$

$$n_6 = 13 + 40 * n_r + 42 * n_r{}^2 + 28 * n_r{}^3$$

$$n_7 = 31 + 78 * n_r + 78 * n_r{}^2$$

$$n_8 = 57 + 189 * n_r + 225 * n_r{}^2 + 150 * n_r{}^3$$

$$n_9 = 31 + 109 * n_r + 141 * n_r{}^2 + 94 * n_r{}^3$$

$$c_4 = 2 * m^* * \omega$$

$$e_1 = \epsilon_1/\sqrt{c_4}$$

$$e_2 = \epsilon_2/c_4$$

$$e_3 = \epsilon_3/c_4{}^{3/2}$$

$$e_4 = \epsilon_4/c_4{}^2$$

$$d_1 = \delta_1/\sqrt{c_4}$$

$$d_2 = \delta_2/c_4$$

$$d_3 = \delta_3/c_4{}^{3/2}$$

$$d_4 = \delta_4/c_4{}^2$$

$$d_5 = \delta_5/c_4{}^{5/2}$$

$$d_6 = \delta_6/c_4{}^3$$

also:

$$\epsilon_1 = c_2/(2 * m^*)$$

$$\epsilon_2 = -\, 3 * c_2/(4 * m^*)$$

$$\epsilon_3 = -\, 1/(2 * m^*) + \left(r_5 * \mathrm{der}_3\,(r)\right)/(6 * Q)$$

$$\epsilon_4 = 5/(8 * m^*) + \left(r_6 * \mathrm{der}_4\,(r)\right)/(24 * Q)$$

$$\delta_1 = -\, c_1 * c_3/(4 * m^*)$$

$$\delta_2 = 3 * c_1 * c_3/(8 * m^*)$$

$$\delta_3 = c_2/m^*$$

$$\delta_4 = -\, 5 * c_2/(4 * m^*)$$

$$\delta_5 = -\, 3/(4 * m^*) + \left(r_7 * \mathrm{der}_5\,(r)\right)/(120 * Q)$$

$$\delta_6 = 7/(8 * m^*) + \left(r_8 * \mathrm{der}_6\,(r)\right)/(720 * Q)$$

where:

$$\mathrm{der}_1\,(r) = \frac{\mathrm{dV}}{\mathrm{dr}}$$

$$\mathrm{der}_2\,(r) = \frac{d^2\mathrm{V}}{\mathrm{dr}}$$

$$\mathrm{der}_3\,(r) = \frac{d^3\mathrm{V}}{\mathrm{dr}}$$

$$\mathrm{der}_4\,(r) = \frac{d^4\mathrm{V}}{\mathrm{dr}}$$

$$\mathrm{der}_5\,(r) = \frac{d^5\mathrm{V}}{\mathrm{dr}}$$

$$\mathrm{der}_6\,(r) = \frac{d^6\mathrm{V}}{\mathrm{dr}}$$

References

[1] Eftekhari, A., J. Mater. Chem. A, 5 (35) (2017) 18299.

[2] Splendiani, A., Sun, L., Zhang, Y., Li, T., Kim, J., Chim, C.Y., Galli, G., and Wang, F., Nano Lett., 10 (4) (2010) 1271.

[3] Radisavljevic, B., Radenovic, A., Brivio, J., Giacometti, V., and Kis, A., Nat. Nanotechnol., 6 (3) (2011) 147.

[4] Shinn, E., Complexity, 18 (3) (2012) 24.

[5] Elishakoff, I., Pentaras, D., Dujat, K., Versaci, C., Muscolino, G., Storch, J., Bucas, S., Challamel, N., Natsuki, T., Zhang, Y.Y., Wang, C.M., and Ghyselinck, G., "Carbon Nanotubes and Nano Sensors: Vibrations, Buckling, and Ballistic Impact", (ISTE-Wiley, London, 2012), XIII+421 pp.

[6] Husain, S., Kumar, A., Kumar, P., Kumar, A., Barwal, V., Behera, N., Choudhary, S., Svedlindh, P., and Chaudhary, S., Phys. Rev. B, 98 (18) (2018) 180404.

[7] Husain, S., Kumar, A., Kumar, P., Kumar, A., Barwal, V., Behera, N., Choudhary, S., Svedlindh, P., and Chaudhary, S., Phys. Rev. B, 98 (18) (2018) 180404.

[8] Mak, K.F., He, K., Shan, J., and Heinz, T.F., Nat. Nanotechnol., 7 (8) (2012) 494.

[9] Zeng, H., Dai, J., Yao, W., Xiao, D., and Cui, X., Nat. Nanotechnol., 7 (8) (2012) 490.

[10] Malic, E. et al., Nat. Commun., 14 (1) (2023) 3430.

[11] Combescot, M. and Shiau, S.-Y., "Excitons and Cooper Pairs: Two Composite Bosons in Many-Body Physics", (Oxford University Press, 2015).

[12] Eftekhari, A., J. Mater. Chem. A, 5 (35) (2017) 18299.

[13] Elsaid, M., Physica B, 202 (1994) 202.

[14] Nie, Z. et al., Commun. Phys., 2 (1) (2019) 103.

[15] Malic, E. et al., Nat. Commun., 14 (1) (2023) 3430.

[16] Combescot, M. and Shiau, S.-Y., "Excitons and Cooper Pairs: Two Composite Bosons in Many-Body Physics", (Oxford University Press, 2015).

[17] Frenkel, J., Phys. Rev., 37 (1) (1931) 17.

[18] Jiles, D., "Introduction to Magnetism and Magnetic Materials", 3rd ed., (Boca Raton, 2015).

[19] Gonano, C.A., Zich, R.E., and Mussetta, M., Prog. Electromagn. Res. B, 64 (2015) 83.

[20] Wannier, G., Phys. Rev., 52 (3) (1937) 191.

[21] Nawaz, S. and Tahir, M., Physica E, 76 (2016) 169.

[22] Han, S.A., Bhatia, R., and Kim, S.-W., Nano Converg., 2 (1) (2015) 17.

[23] Nguyen, D.-A.P. et al., Physica E, 113 (2019) 152.

[24] Keldysh, L.V., Sov. J. Exp. Theor. Phys. Lett., 29 (1979) 658.

[25] Cudazzo, P., Tokatly, I.V., and Rubio, A., Phys. Rev. B, 84 (8) (2011) 085406.

[26] Sarkar, S., Sarkar, S., and Bose, C., Physica B, 541 (2018) 75.

[27] Liang, S.J. and Xie, W.F., Eur. Phys. J. B, 81 (1) (2011) 79.

[28] Sukhatme, U. and Imbo, T., Phys. Rev. D, 28 (2) (1983) 418.

[29] Imbo, T., Pagnamenta, A., and Sukhatme, U., Phys. Rev. D, 29 (8) (1984) 1669.

[30] Baghdasaryan, D.A. et al., Physica E, 101 (2018) 1.

[31] Nawaz, S. and Tahir, M., Physica E, 76 (2016) 169.

[32] Shaer, A.A.A., "The Gaussian Impurity Effect on the Electronic and Magnetic Properties of an Electron Confined in a Lateral Quantum Dot", (2023).

[33] Gschneidner, K.A. Jr. and Pecharsky, V.K., Annu. Rev. Mater. Sci., 30 (2000) 387.

[34] Pecharsky, V.K. and Jr. Gschneidner, K.A., J. Magn. Magn. Mater., 200 (1999) 44.

[35] Svensson, J., "A Study of the Magnetic Properties of Yb_4LiGe_4: Unusual Magnetism", (Diss., Boston College, 2010).

[36] Ma, N. and Reis, M.S., Sci. Rep., 7 (1) (2017) 13257.

[37] Cortés, N. et al., Phys. Rev. B, 105 (1) (2022) 014443.